Scattering Manipulation and Camouflage of Electrically Small Objects through Metasurfaces

S. Vellucci,[1,*] A. Monti,[2] A. Toscano,[1] and F. Bilotti[1]

[1]"Roma Tre" University, Department of Engineering, Via Vito Volterra 62, 00146 Rome, Italy
[2]Niccolò Cusano University, Via don Carlo Gnocchi 3, 00166 Rome, Italy

(Received 6 September 2016; revised manuscript received 25 February 2017; published 28 March 2017)

In this paper, we discuss the intriguing possibility of tailoring the scattering response of an electrically small object for camouflage and illusion applications using metasurfaces. As a significant example, we focus our attention on the cylindrical geometry and derive the analytical conditions needed to camouflage the geometrical and electrical characteristics of dielectric and metallic cylinders coated with ideal metasurfaces. A closed-form expression of the camouflaging metasurface depending on the cylinder's characteristics is derived. Furthermore, the frequency behavior and the limitations of this technique are discussed with the aid of relevant examples. In order to overcome these limitations, a solution based on the use of lossy metasurfaces is proposed.

DOI: 10.1103/PhysRevApplied.7.034032

I. INTRODUCTION

One of the most exciting and promising applications enabled by metamaterials is represented by the invisibility cloaks [1–5], i.e., devices that are able to reduce the electromagnetic visibility of an object by minimizing its total scattering cross section (SCS) in a given frequency range. The effectiveness of electromagnetic cloaks has been experimentally proven in several scenarios [6–8] and for different fascinating applications ranging from low observability in antennas and defense systems [9–14] to noninvasive sensing [15] at both radio and optical frequencies [16]. In all these cases, the cloaking effect is achieved through the use of covers that exploit the anomalous interaction between the electromagnetic wave and the metamaterial cloak, leading to an overall minimization of the scattering signature of the object.

The transformation-optics technique [1] is based on a transformation of the space surrounding the object enabled by inhomogeneous and anisotropic bulk metamaterials. Such a transformation is able to bend the incident electromagnetic field around the object to hide, making the inner region of the cloak effectively invisible to any external excitations. Despite its theoretical impact, the stringent requirements of the metamaterial cover make the effective implementation of this technique very challenging for its extreme sensitivity to both fabrication imperfections and electromagnetic losses [3]. Furthermore, the need of a superluminal propagation in the cloak limits the working bandwidth of this solution [5,17]. Finally, we also emphasize that this cloaking approach is impractical for sensing and antenna applications [15] due to the fact that the inner region of the cloak is electromagnetically isolated from the external perturbation.

Conceptually not too dissimilar, the transmission-line cloaking technique [2] uses transmission-line networks to hide objects from electromagnetic waves. In this case, the incident waves are convoyed into a transmission-line network that is tailored to exhibit a very low scattering cross-section, i.e., to be impedance matched to free space. The main advantage of this approach is that a superluminal propagation is not required, and, thus, it is inherently broadband. Moreover, the cloak design and manufacturing is quite straightforward. However, some important limitations for the shape of the cloaked object apply, and, moreover, the corresponding cloak is a bulky and massive structure.

Conversely, the scattering-cancellation method [3,4] is based on a radically different approach that aims to cancel the dominant Mie scattering coefficients of the cloaked object. The invisibility effect is achieved when the induced dipole moments of the cloak and the object to hide are equal in magnitude but out of phase. One important difference of this technique compared to the transformation optics lies in the fact that the cloaked object is not isolated from the external field. This makes this technique suitable for antennas and sensor applications. Moreover, the design and implementation of the cloaks are quite straightforward since they can be realized using a single layer of homogenous and isotropic materials [18]. As a disadvantage, the scattering-cancellation method is not the best choice for objects that are large compared to the operative wavelength due to the increasing number of scattering terms that comes into play in the description of the scattering response of the object [19].

The implementation of the scattering-cancellation method can be achieved using cloaks made of either bulk plasmonic metamaterials [3] or ultrathin-coating metasurfaces [4]. This latter approach, also known in the literature

*Corresponding author.
stefano.vellucci@uniroma3.it

 © 2017 American Physical Society

as *mantle cloaking*, leads to lightweight, thin, and conformal designs that can be easily implemented at rf, microwaves, and even for acoustic waves [20,21]. In these ranges of frequencies, in fact, a metasurface is implemented through a patterned metallic surface with a subwavelength period that can be modeled using the homogenized physical quantity known as the average surface impedance Zs (Ω/sq), which is the ratio between the tangential component of the electric field and the surface current density. The surface impedance is a complex quantity described by a real and an imaginary part. The first one is due to the losses of the materials composing the metasurface, while the second one describes the energy stored by the structure and, therefore, can assume negative (capacitive) or positive (inductive) values. For lossless structures, as we can safely assume for microwave metasurfaces due to the very high value of the metal conductivity at such frequencies, the surface impedance is a purely imaginary quantity, and, therefore, it is described by its surface reactance X_s (Ω/sq).

So far, mantle cloaking has been demonstrated to be rather versatile, and it has found many applications in the antenna field. However, the possibilities offered by the mantle-cloaking approach, and, more in general, by metasurfaces, go well beyond the minimization of the overall scattered field. The invisibility effect, in fact, can be interpreted as a particular case of a more general manipulation of the scattering properties of a metasurface-coated object. The opportunity for comprehensive control over the electromagnetic scattering properties of an object allows us to transform the scattering properties of a given object into the ones of another different object (e.g., making the object appear as if it were larger or thinner or made by a different material), leading to a camouflage or an illusion effect. This effect is highly desirable in several applications, such as defense security. In particular, it is possible to exploit this effect for inducing confusion in an observing radar through the camouflage of the observed target, even if with possible bandwidth limitations depending on the type of radar technique involved, as we discuss later on. The same approach can be also useful in different applications where, for geometrical or structural reasons, it is not possible to reduce the dimensions of an object whose consequent level of scattering becomes incompatible with the electromagnetic functionalities owned by the object itself.

Recently, some studies based on the use of transformation optics and mantle cloaking to achieve an illusion effect have been developed [22–28]. In particular, in Ref. [26], it has been experimentally demonstrated that an ultrathin anisotropic metasurface can be used to transform the scattering response of a coated dielectric cylinder into the one of an uncoated conducting cylinder and vice versa. In Ref. [27], a similar study is proposed exploiting an active illusion or cloaking coat consisting of an array of magnetic monopoles. Despite these efforts, no closed-form design formulas are available, and, moreover, the camouflage analysis is restricted to a single operative frequency with a consequent limitation on the use of these approaches in real scenarios.

Inspired by these earlier works, in this paper, we propose a systematic analytical methodology for achieving advanced scattering manipulation. Starting from the well-known scattering problem by an infinite cylinder, we show that it is possible by properly tailoring the value assumed by the surface impedance of the coating metasurface in order to achieve a desired level of scattering. Some theoretical and numerical examples are proposed to validate the proposed idea, and, specifically, it is shown that the scattering response of a coated cylinder can be transformed and made equal to the one of a cylinder with different electrical and/or geometrical characteristics. An analysis of the frequency performance that can be theoretically achieved by the camouflage effect is carried out, and some solutions to overcome the intrinsic narrow-band behavior of the illusion effect are also proposed. Compared to the works about this topic [22–28], the results discussed here can be considered as an important step further toward the use of higher-performance camouflage devices in realistic applications.

II. ANALYTICAL FORMULATION OF THE SCATTERING MANIPULATION PROBLEM USING METASURFACES

The basic principle of the camouflage effect we desire to achieve is depicted in Fig. 1 for the case of a cylindrical geometry. In this case, the scattering signature of a cylindrical object (the red cylinder) is transformed into the one of another cylinder (the blue cylinder) with different size and material properties through the use of metasurfaces (the yellow cover around the red cylinder). In order to derive the analytical expression of the required camouflage surface impedance, we need to equate the expressions of the scattering coefficients of the targeted object with the scattering coefficients of the covered object.

To do so, we have to first solve the well-known scattering problem by an infinite dielectric cylinder (hereinafter, *the targeted cylinder*) with radius a_1 and electromagnetic parameter (ε_1, μ_0) as sketched in Fig. 2(a). Then, we have to consider the scattering problem by another cylinder (*coated cylinder*) with radius a_2 and electromagnetic

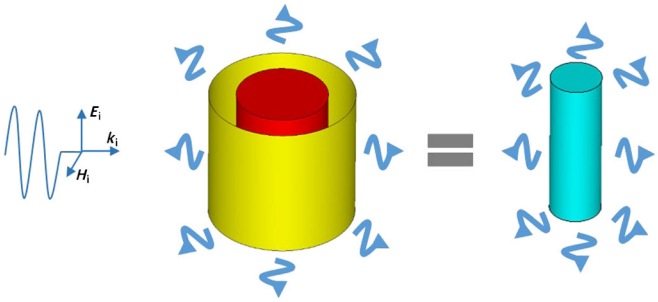

FIG. 1. Sketch of the working principle of the camouflaging metasurface.

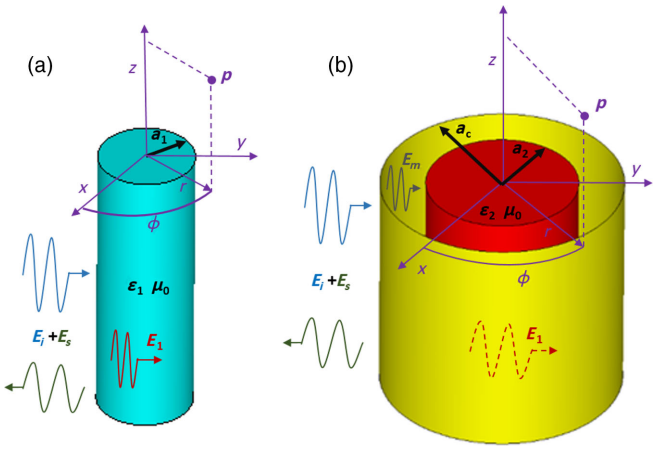

FIG. 2. Geometry of the scattering problem by (a) a dielectric cylinder and (b) by a metasurface-coated dielectric cylinder.

parameters (ε_2, μ_0) and surrounded by an ultrathin ideal metasurface with radius a_c [Fig. 2(b)].

We assume that the cylinders are illuminated by an external normally incident plane wave with transverse-magnetic (TM) polarization (i.e., with the electric field parallel to the cylinder axis). Using a cylindrical reference system (r, ϕ, z) and adopting a standard Mie expansion [29], we can write the incident electric field $(\boldsymbol{E}_i)$, the scattered electric field $(\boldsymbol{E}_s)$, and the electric field inside the dielectric cylinder $(\boldsymbol{E}_1)$ as

$$\begin{aligned}\boldsymbol{E}_i &= \sum_{n=-\infty}^{\infty} E_n \mathbf{N}_n^{(1)}(r,\phi,z),\\ \boldsymbol{E}_1 &= \sum_{n=-\infty}^{\infty} E_n [c_n \mathbf{M}_n^{(1)} + d_n \mathbf{N}_n^{(1)}],\\ \boldsymbol{E}_s &= -\sum_{n=-\infty}^{\infty} E_n [b_n \mathbf{N}_n^{(3)} + j a_n \mathbf{M}_n^{(3)}],\end{aligned} \tag{1}$$

where the magnetic field components can be derived as $\boldsymbol{H} = -j/\omega\mu_0 \nabla \times \boldsymbol{E}$, and the expression of $\mathbf{N}_n(r,\phi,z)$, $\mathbf{M}_n(r,\phi,z)$ can be found in Ref. [29]. In Eq. (1), the scattered field is conveniently expressed as the discrete sum of cylindrical harmonics with complex amplitudes a_n and b_n (with n being an integer and $a_{-n} = -a_n$, $b_{-n} = -b_n$). Please note that since these coefficients are the amplitude of the transverse-electric (TE) and transverse-magnetic (TM) cylindrical waves, they are also known in the literature as c_n^{TE} and c_n^{TM} [3].

The coefficients a_n and b_n describing the electromagnetic field scattered by the cylinder are related to the total scattering efficiency of the object. In particular, the scattering cross section per unit length of an infinite cylinder can be expressed as [29]

$$Q_{\mathrm{sca}} = \frac{2}{x}\left[|b_0|^2 + 2\sum_{n=1}^{\infty}(|b_n|^2 + |a_n|^2)\right], \tag{2}$$

where $x = ka_1$, and k is the wave number. The total scattering efficiency Q_{sca} is a sum of infinite terms. However, in the case of electrically small objects, the scattering coefficients above the fundamental order are negligible [29]; i.e., the scattered field is dominated by the first-order mode. The number n of the terms that effectively contribute to the total efficiency usually increases with the physical or electrical size of the scatterer, and this is one of the reasons why larger objects generally scatter more.

To determine the analytical expressions of the scattering coefficients in the scenario depicted in Fig. 2(a), it is sufficient to enforce the boundary conditions for the tangential components of the electric and magnetic fields at the interface $r = a_1$ of the cylinder. In this way, it is possible to derive a compatible equation system whose analytical solution returns the unknown amplitude coefficients. In particular, for the case of the normally incident TM-plane wave, the scattering coefficients a_n are identically zero, and, for electrically small cylinders, we can safely consider only the first term of the scattering series (b_0). Moreover, the expression of the scattering coefficient available in the literature [29] can be further simplified by applying the asymptotic expansion of the Bessel functions for small arguments [30], obtaining, thus, the following expression:

$$\begin{aligned}b_0 &= \frac{J_0(a_1k_0\sqrt{\varepsilon_1})J_1(a_1k_0) - \sqrt{\varepsilon_1}J_0(a_1k_0)J_1(a_1k_0\sqrt{\varepsilon_1})}{J_0(a_1k_0\sqrt{\varepsilon_1})H_1^{(1)}(a_1k_0) - \sqrt{\varepsilon_1}J_1(a_1k_0\sqrt{\varepsilon_1})H_0^{(1)}(a_1k_0)}\\ &\cong -\frac{j\pi a_1^2 k_0^2(\varepsilon_1 - 1)}{2a_1^2k_0^2\varepsilon_1 \ln(a_1k_0) + 4},\end{aligned} \tag{3}$$

where J_n $(n = 0, 1)$ is the n*th*-order cylindrical Bessel function of the first kind, $H_n^{(1)}$ $(n = 0, 1)$ is the n*th*-order cylindrical Hankel function of the first kind, and k_0 is the free-space wave number.

In a similar way, it is possible to derive the expressions for a coated dielectric cylinder [see Fig. 2(b)]. The analytical expressions of the incident, scattered, and inner electric fields are the same as in Eq. (1), but, in this case, a field inside the shell is also present between the surfaces of the inner cylinder and the outer metasurface $(\boldsymbol{E}_m)$:

$$\begin{aligned}\boldsymbol{E}_i &= \sum_{n=-\infty}^{\infty} E_n \mathbf{N}_n^{(1)}(r,\phi,z),\\ \boldsymbol{E}_1 &= \sum_{n=-\infty}^{\infty} E_n [c_n' \mathbf{M}_n^{(1)} + d_n' \mathbf{N}_n^{(1)}],\\ \boldsymbol{E}_m &= \sum_{n=-\infty}^{\infty} E_n [j e_n' \mathbf{N}_n^{(3)} + j e_n'' \mathbf{N}_n^{(1)} - f_n' \mathbf{M}_n^{(3)} - f_n'' \mathbf{M}_n^{(1)}],\\ \boldsymbol{E}_s &= -\sum_{n=-\infty}^{\infty} E_n [b_n' \mathbf{N}_n^{(3)} + j a_n' \mathbf{M}_n^{(3)}],\end{aligned} \tag{4}$$

where a_n', b_n', c_n', d_n', e_n', f_n', e_n'', f_n'' are the new unknown amplitude coefficients. By enforcing the continuity of the

tangential components of the electric and magnetic fields at $r = a_2$ and the boundary condition of an *ideal electrically polarizable metasurface* at the boundary $r = a_c$ [4], i.e., $\boldsymbol{E}_{\boldsymbol{m}}^{\tan} = Z_s\hat{\boldsymbol{r}}[(\boldsymbol{H}_{\boldsymbol{i}}^{\tan} + \boldsymbol{H}_{\boldsymbol{s}}^{\tan}) - \boldsymbol{H}_{\boldsymbol{m}}^{\tan}]$, it is possible to derive the exact analytical expressions of the scattering coefficients b_n'. As for the previously discussed case of the uncoated cylinder, we assume that the coated cylinder is electrically small, i.e., $k_0 a_c \ll 1$ and $k_c a_c \ll 1$ (where k_0 and k_c are the wave numbers in free space and in the shell, respectively). Therefore, we can safely consider only the first term of the scattering series (b_0') [3], and by applying the asymptotic expansion of the Bessel functions for small arguments once again, b_0' reduces to (see Appendix A for details)

$$b_0' \cong \frac{\pi\{a_2^2 a_c k_0^2 \mu_0 \omega[\varepsilon_2 \ln(\frac{a_2}{a_c}) + \ln(a_c k_0)] - j a_2^2 k_0^2 Z_s(\varepsilon_2 - 1) + 2a_c\mu_0\omega\}}{2a_2^2 k_0^2 \varepsilon_2 \ln(a_2 k_0)[Z_s + j a_c \mu_0 \omega \ln(a_c k_0)] + 2a_c \ln(a_c k_0)[-j a_2^2 k_0^2 \mu_0 \omega(\varepsilon_2 - 1)\ln(a_c k_0) + a_c k_0^2 Z_s + 2j\mu_0\omega] + 4Z_s}. \quad (5)$$

It is worth noticing that the scattering coefficient b_0' depends on the geometrical and electromagnetic parameters of the overall structure and on the surface impedance Z_s. Once the analytical expression of the complex Mie scattering coefficients of the coated cylinder b_0' and the one of the targeted cylinder b_0 are found, it is possible to derive the analytical expression of the surface impedance needed to achieve the camouflage effect by equating the two scattering coefficients. In particular, the expression of Z_s that allows us to make the two scattering coefficients equal in both the imaginary and real parts is

$$Z_s \cong jX_s \cong j\frac{2a_c\mu_0\omega\{a_1^2k_0^2[\varepsilon_1 \ln(\frac{a_1}{a_c}) + \ln(a_c k_0)] + 2\}\{a_2^2 k_0^2[\varepsilon_2 \ln(\frac{a_2}{a_c}) + \ln(a_c k_0)] + 2\}}{k_0^2[a_2^2 k_0^2 \ln(a_c k_0) + 2]\{a_1^2 a_2^2 k_0^2[\varepsilon_1(\varepsilon_2 - 1)\ln(a_1 k_0) - \varepsilon_2(\varepsilon_1 - 1)\ln(a_2 k_0)] + 2[a_2^2(\varepsilon_2 - 1) - a_1^2(\varepsilon_1 - 1)]\}}, \quad (6)$$

where a_1 and ε_1 are the geometrical and electrical parameters of the targeted cylinder, while a_2, ε_2, and a_c are the parameters of the coated cylinder. It is interesting to note that the value of Z_s is purely reactive and that if $\varepsilon_1 = \varepsilon_2$ and $a_1 = a_2$ (i.e., the targeted cylinder and the coated cylinder are the same object), the surface impedance approaches $-j\infty$, as expected, suggesting the absence of the metasurface. As can be easily inferred, the same result is obtained also in the case $\varepsilon_1 = \varepsilon_2 = 1$ (i.e., in the absence of both cylinders).

An analogous expression can be easily obtained also for the case of conducting cylinders by calculating the limit of Eq. (6) as the cylinder permittivity approaches $-j\infty$. Similar analytical results can also be obtained for other canonical geometries, such as the spherical or the ellipsoidal one. For noncanonical shapes for which the closed-form solution of the scattering problem does not exist, numerical approximations [31] can be used for achieving a semianalytical design.

Interestingly, the availability of an analytical expression for the camouflage surface impedance allows the analysis of its frequency behavior. From a physical point of view, the mechanism behind the camouflage effect is similar to the one of mantle cloaking: the surface currents supported by the metasurface are engineered to interfere properly with the fields naturally induced by the bare object, giving rise to the altered scattered fields. The important difference is that, in the case of camouflage, the goal is more challenging than the simple minimization of the first-order scattering coefficient since the aim is to achieve a given level of the total scattering.

As known in Ref. [32], the intrinsic bandwidth limitations of the cloaking effect are due to Foster's reactance theorem, and an increase of the operational bandwidth necessarily requires active loads. We expect the same bandwidth behavior in the case of camouflage, at least for the cases of reduction of the scattering amplitude of the coated object. This behavior is confirmed by Fig. 3, where some significant cases of the frequency behavior of Eq. (6) are reported. It is interesting to notice that there are some scenarios where the camouflaging surface reactance exhibits a Foster response; i.e., the surface reactance *increases* as the frequency

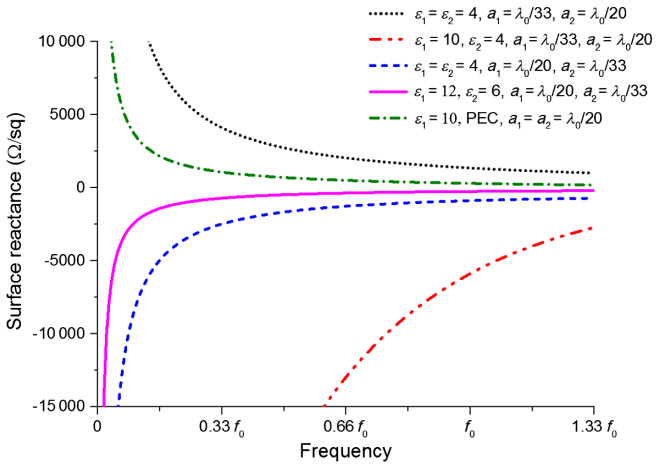

FIG. 3. Frequency behavior of the camouflage condition (6) for some significant cases.

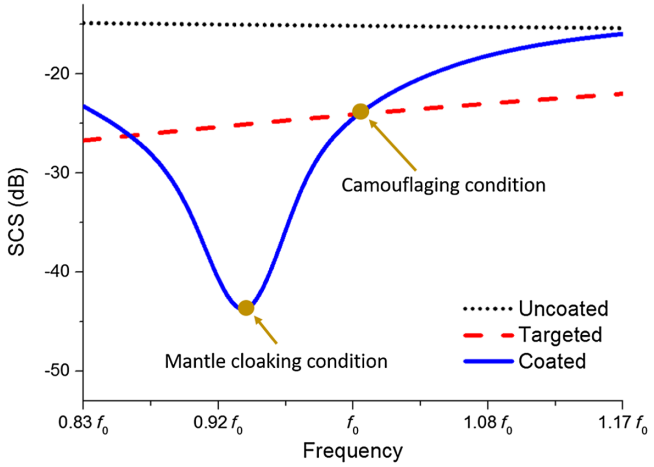

FIG. 4. Analytical SCS of PEC (bare), dielectric (targeted), and camouflaged cylinder. The geometrical and electrical characteristics used for this example are $a_1 = a_2 = \lambda_0/20$, $a_c = 1.5a$, and $\varepsilon_r = 4$.

increases. Specifically, these scenarios appear when $a_1 > a_2$ or $\varepsilon_1 > \varepsilon_2$; i.e., when we desire to increase the scattering of the bare object to make it appear as if it were larger or realized with electromagnetically denser materials. In the following sections, we provide more physical insights into the camouflage possibilities by showing the analytical and full-wave results of some significant examples.

III. SCATTERING REDUCTION

To demonstrate the versatility of the general approach, in this section, we present some examples showing how a metasurface-coated infinite cylinder can match the scattering properties of another one with different electromagnetic and geometrical characteristics. As a first case, we consider a coated infinite conducting cylinder designed to behave as an infinite dielectric cylinder with the same physical size. This case is somehow similar to the invisibility one, where it is desirable to minimize the scattering signature of the object. However, in our case, we want to achieve a specific level of the scattering signature of the coated object and not its generic minimization.

We consider a cylinder made of a perfect electric conductor (PEC) with radius $a_2 = \lambda_0/20$ and a targeted dielectric cylinder with the same radius $a_1 = \lambda_0/20$ and $\varepsilon_1 = 4$, being λ_0 the wavelength at the camouflage frequency f_0. By using an ideal ultrathin metasurface, the camouflage effect can be achieved with a metasurface that has a radius $a_c = 1.5a_2$ and surface impedance equal to $-j65\ \Omega/\mathrm{sq}$, according to Eq. (6). Please note that the radius of the coating metasurface is chosen in order to still satisfy the quasistatic condition we use above for deriving Eq. (6).

In Fig. 4, we report the SCS of the targeted, coated, and bare cylinders as the frequency changes. These curves are evaluated by solving the analytical problem that we discuss in the previous section. As can be appreciated, an ideal nondispersive metasurface with surface impedance $Z_s = -j65\ \Omega/\mathrm{sq}$ allows us to achieve the camouflage condition at the design frequency f_0. It is interesting to note that, apparently, a second camouflage condition seems to exist around $0.86f_0$. This solution that is not predicted by Eq. (6) arises from the fact that the SCS is directly related to the magnitude of the scattering coefficients and that there are two distinct values of Z_s for which the equation $|b_0| = |b_0'|$ applies. However, the second solution implies only an equivalence of the magnitude but not of the phase of the scattered waves and, therefore, does not yield to cylinders with identical scattering response ($b_0 \neq b_0'$). Therefore, for camouflage applications, this second solution is not of interest since the camouflaged object can still be detectable from the phase distribution of the scattered electromagnetic field that is different from the expected one (see Appendix B for details).

Finally, it is also worth noticing that as predicted from the analysis on the physical phenomena at the basis of the camouflage effect, the coated cylinder also exhibits a

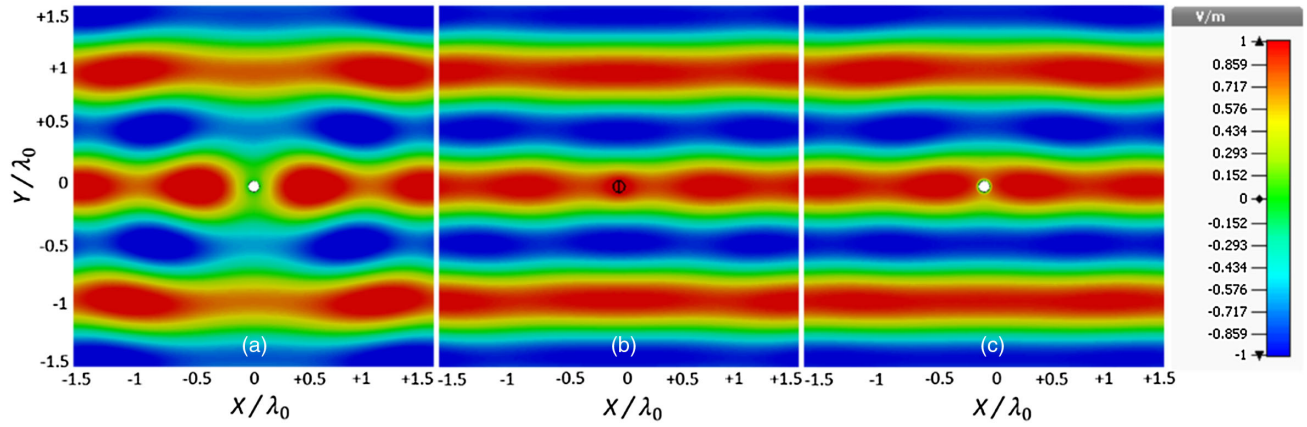

FIG. 5. Magnitude of the electric field distribution at f_0 on a plane perpendicular to the cylinder axis of the (a) bare, (b) targeted, and (c) camouflaged cylinder evaluated using full-wave simulations.

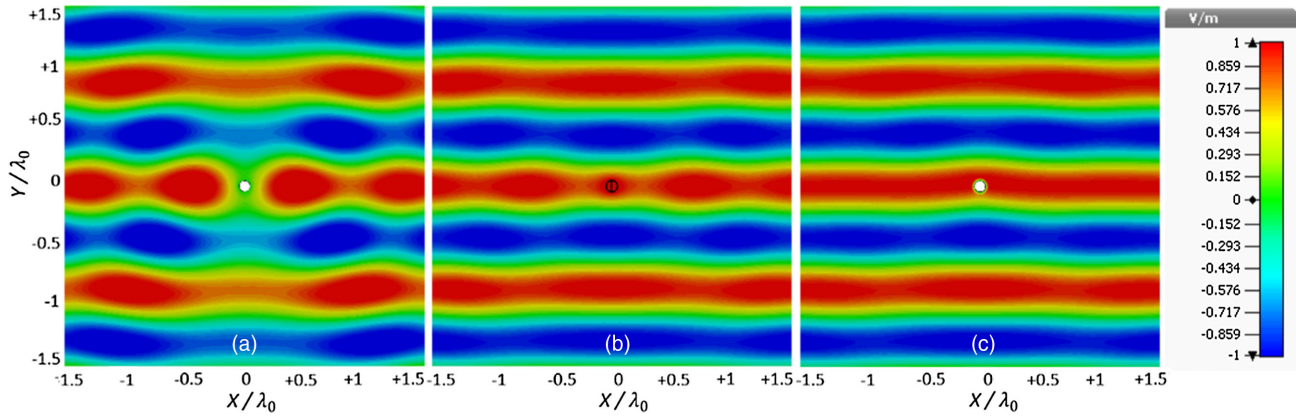

FIG. 6. Magnitude of the electric field distribution at $0.94f_0$ on a plane perpendicular to the cylinder axis of the (a) bare, (b) targeted, and (c) cloaked cylinder evaluated using full-wave simulations.

minimum scattering condition (in particular, for this specific case, it occurs around $0.94f_0$).

To confirm the analytical results, in Fig. 5 we compare the near-field electric field distributions of the bare [Fig. 5(a)], targeted [Fig. 5(b)], and camouflaged [Fig. 5(c)] infinite cylinder for a normally incident plane-wave excitation obtained through full-wave simulations [33]. As expected, the designed metasurface is able to produce almost the same field distribution of the targeted cylinder in terms of magnitude and spatial distribution. It is also interesting to observe that the field is able to penetrate the area between the metasurface and the PEC cylinder, indicating that the conductor is not electromagnetically isolated from the external world.

As we remark in the theoretical analysis, the intrinsic frequency dependence of the SCS also allows us to achieve a mantle-cloaking condition at a slightly different frequency than f_0. This effect is shown in Fig. 6, where it is possible to appreciate the restoration of the plane-wave phase front in the cloaked case.

To conclude this section, in Fig. 7, we show the E-field distributions for several frequencies close to the

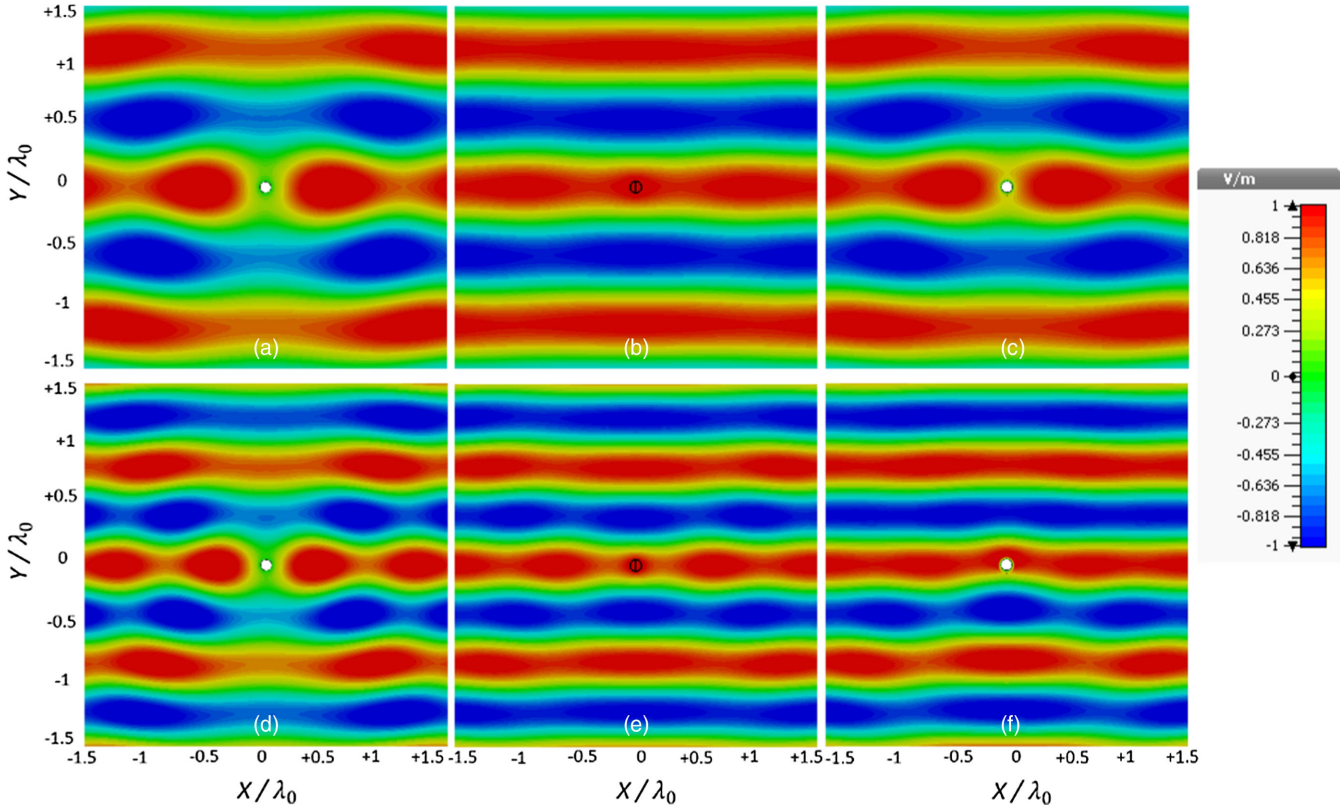

FIG. 7. Magnitude of the electric field distribution on a plane perpendicular to the cylinder axis of the (a),(d) bare, (b),(e) targeted, and (c),(f) camouflaged cylinder evaluated using full-wave simulations at [(a)–(c)] $0.83f_0$ and at [(d)–(f)] $1.17f_0$.

camouflaged one. As expected, the illusion effect is quite narrowband due to the intrinsic Foster behavior of the passive camouflaging metasurface that is able to meet the camouflaging condition (6) only at one frequency.

In Sec. V, we propose a possible solution for increasing the bandwidth of the camouflaging effect based on the use of lossy metasurfaces.

IV. SCATTERING ENHANCEMENT

To further emphasize more versatility of the camouflage approach compared to cloaking, we show in this section how a metasurface can be designed to enhance a weak scattering response and make an object appear as if it were a stronger scatterer. In this case, the targeted object is a dielectric cylinder with relative permittivity $\varepsilon_1 = 12$ and radius $a_1 = \lambda_0/20$, whereas the coated cylinder has relative permittivity $\varepsilon_2 = 6$ and radii $a_2 = \lambda_0/33.3$ and $a_c = 1.5a_2$. Please note that the overall radius of the coated structure is smaller than the targeted one, even considering the presence of the coating metasurface. Moreover, to demonstrate the flexibility of the proposed method, we consider here finite-length cylinders with length equal to $4\lambda_0$, which is a reasonable length to consider still valid for the analytical formulas that we derive above. The value of the surface impedance needed to achieve the camouflage effect is first calculated using Eq. (6) ($Z_s = -j210.33\ \Omega/\mathrm{sq}$) and then slightly optimized with a *full-wave simulator* in order to take into account the finite size of the objects ($Z_s = -j200\ \Omega/\mathrm{sq}$).

Figure 8 compares the 3D scattering cross section in the three cases under a normally incident TM-plane-wave excitation. It can be seen that the coated cylinder exhibits a scattered field distribution very similar to the one of the targeted cylinder. This additional case confirms that a properly engineered single-layer metasurface can be designed to effectively transform the scattering signature of an object into that of another that can be either a weaker or a stronger scatterer.

To analyze the frequency behavior of the scattering enhancement metasurface, we decide to implement a real metasurface having the specific value of the surface impedance needed to achieve the camouflage behavior at the design central frequency, i.e., $Z_s = -j200\ \Omega/\mathrm{sq}$. The required metasurface is capacitive, and, therefore, it can be implemented using a horizontal-strip metasurface. Using the design formulas available in Ref. [18], we can easily obtain the geometrical values of the metasurface that have a gap $g = 18$ mm and a period $D = 50$ mm. The metasurface shown in Fig. 9(b) is composed of eight copper metallic rings placed around the cylinder to be coated and is designed to operate at $f_0 = 3$ GHz.

The full-wave SCS as the frequency changes is reported in Fig. 9(a) for the cases of bare, targeted, analytically coated, and realistically coated cylinders. The analytical metasurface used for the comparison is a mathematical sheet whose surface impedance is equal, frequency by frequency, to the camouflaging conditions expressed by Eq. (6). As can be appreciated, and different from the scattering-reduction case that we analyze in the previous section, the coated object is able to achieve the scattering level of the targeted one in a very broad frequency range. As predicted at the end of Sec. II, this is due to the Foster-like frequency behavior of the camouflaging metasurface required in the scattering-enhancement scenario that is well matched by the designed metasurface [18]. Moreover, we also observe an excellent agreement between the SCS of the real and analytical metasurfaces. At higher frequency, an increasing mismatch between the two curves can be observed. This is an expected effect, and it is due to the fact that the analytical formulation is based on the assumption of small arguments of the Bessel functions and that it is progressively violated as the frequency increases. For more details about this aspect, please refer to Appendix A.

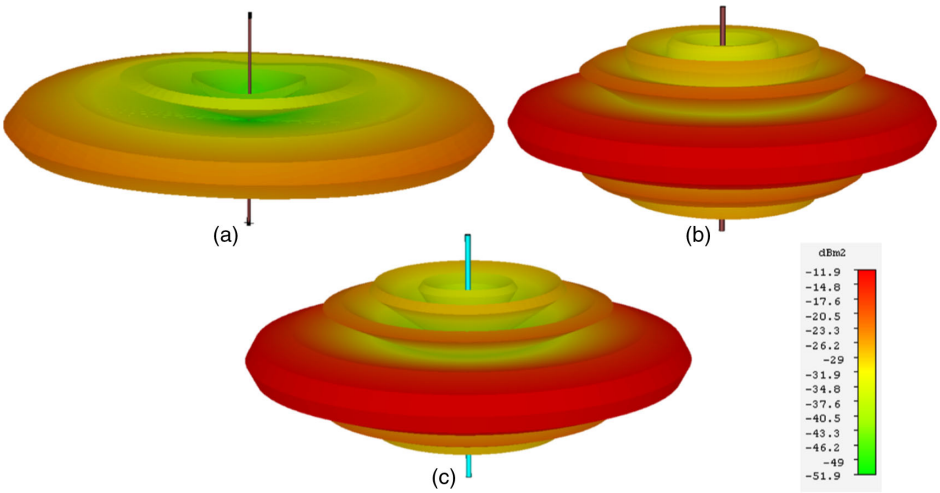

FIG. 8. 3D scattering cross section at f_0 of the (a) uncoated, (b) targeted, and (c) camouflaged cylinder evaluated through full-wave simulations.

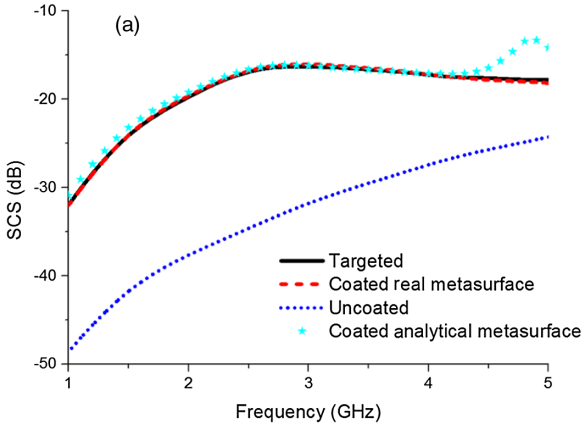

FIG. 9. (a) SCS of the bare, targeted, analytically coated, and realistically coated cylinders. (b) Details of the metasurface. The electrical and geometrical parameters used for this example are $a_1 = \lambda_0/20$, $a_2 = \lambda_0/33.3$, $a_c = 1.5a_2$, $\varepsilon_1 = 12$, $\varepsilon_2 = 6$.

V. LOSSY METASURFACES

In this section, we investigate a possible solution that can be used to improve the frequency performance of the scattering-reduction approach that we analyze in Sec. III. As discussed in Ref. [4], the minimization of the absolute value of the scattering coefficient requires the use of the lossless metasurface whose surface impedance is a purely imaginary quantity. In other terms, the presence of Ohmic losses severely limits the performance of an invisibility device.

As we stress above, in the camouflage approach, we do not aim for a total reduction of the visibility of an object but to its manipulation. In this situation, we can force the minimization of the fundamental Mie coefficient of the covered object by properly tailoring both the imaginary and real parts of the surface impedance in order to achieve the desired level of the scattering coefficient. Such a new degree of freedom allows us to flatten the invisibility resonance, or, from a different point of view, increase the operative bandwidth of the camouflage effect.

In order to analytically determine the required lossy surface impedance, we need to slightly modify the analytical procedure used so far. The first step is to derive the cloaking surface reactance needed to achieve a *minimum scattering condition* in the response of the coated cylinder. To do so, it is possible to use Eq. (6) with $\varepsilon_1 = 1$. Once the optimal cloaking surface reactance (X_s^{cloaking}) is derived, we need to introduce a real part R_s in the surface impedance ($Z_s = R_s + jX_s^{\text{cloaking}}$) and determine the value of R_s which allows us to achieve the desired level of the scattering coefficient at the operation frequency f_0. To do so, it is possible to equate the two scattering coefficients b_0 and b_0' similar to how we derive Eq. (6) but with the important difference that the surface impedance now also includes a real part.

To better explain this concept, let us consider, as an example, a coated dielectric cylinder and a targeted dielectric cylinder with relative permittivity $\varepsilon_1 = \varepsilon_2 = 10$ and radius $a_1 = \lambda_0/33.3$, $a_2 = \lambda_0/20$, and $a_c = 1.5a_2$, respectively. First, we have to analytically determine the lossless surface impedance required to achieve a cloaking condition. We obtain $jX_s^{\text{cloaking}} = j253\ \Omega/\text{sq}$. Then, we need to determine the real part of the surface impedance needed to achieve the desired level of scattering. Equating the two scattering coefficients and imposing $Z_s = R_s + j253\ \Omega/\text{sq}$, we obtain $R_s = 137\ \Omega/\text{sq}$. In Fig. 10, we report the analytical scattering cross sections at f_0 of the targeted, bare, and cloaked cylinders as a function of the real part R_s of the coating surface impedance. As can be appreciated, the introduction of a specific amount of loss allows us to flatten the invisibility condition, thus, transforming the cloaking cover into a broadband camouflaging one.

In Fig. 11, we report some full-wave simulations confirming the bandwidth improvement returned by this technique. The coated cylinder is surrounded with both an optimal lossless camouflaging metasurface with surface reactance $Z_s = j369\ \Omega/\text{sq}$, designed using Eq. (A6), and different lossy metasurfaces ($Z_s = R_s + jX_s^{\text{cloaking}} = Z_s = R_s + j253\ \Omega/\text{sq}$). The optimal lossy metasurface,

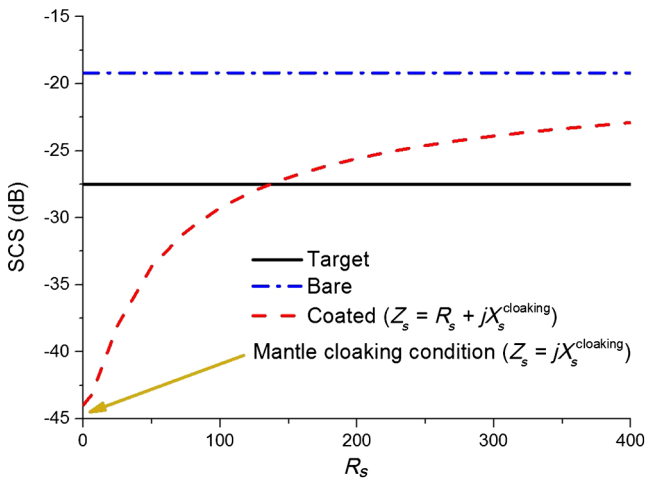

FIG. 10. Basic principle of lossy camouflaging. Analytically evaluated SCS of a bare, targeted, and coated with a tailored lossy metasurface cylinder. The electrical and geometrical parameters used for this example are $a_1 = \lambda_0/33.3$, $a_2 = \lambda_0/20$, $a_c = 1.5a_2$, $\varepsilon_1 = \varepsilon_2 = 10$.

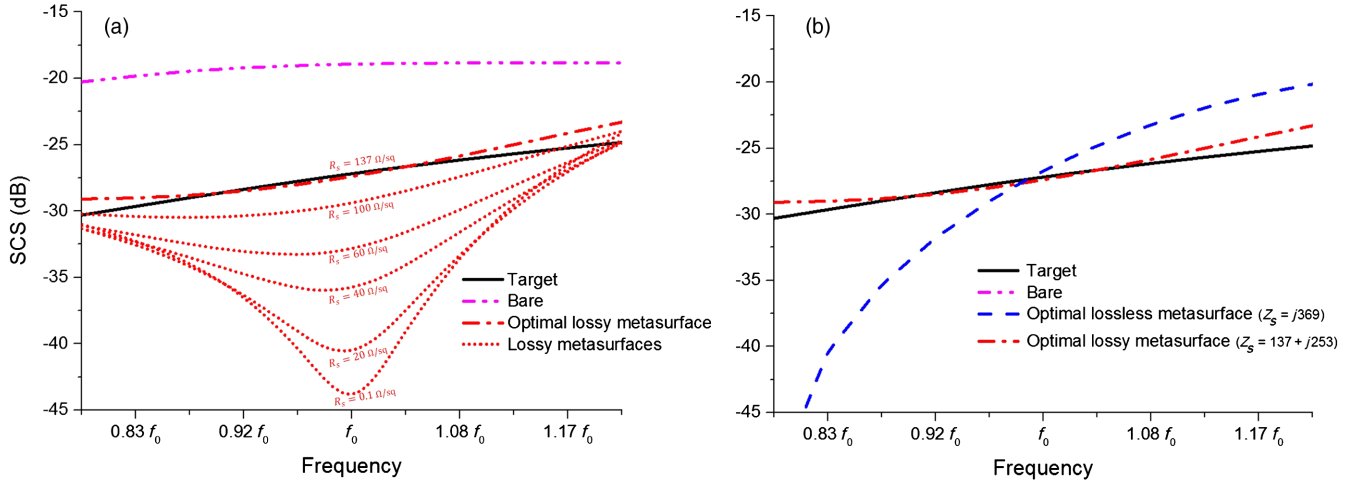

FIG. 11. Camouflage performance of lossless and lossy metasurfaces evaluated through full-wave simulations ($a_1 = \lambda_0/20$, $a_2 = \lambda_0/33.3$, $a_c = 1.5a_1$, $\varepsilon_1 = \varepsilon_2 = 10$). In (a), the performance of lossy metasurfaces is reported for different values of the surface resistance R_s (from 0.1 to 137 Ω/sq). In (b) a comparison between the performance of the optimal lossless ($Z_s = j177$ Ω/sq) and optimal lossy ($Z_s = 137 + j253$ Ω/sq) metasurfaces is shown.

whose performance is depicted with the dot-dashed line, corresponds to a surface impedance equal to $Z_s = 137 + j253$ Ω/sq.

As can be appreciated in Fig. 11(b), the optimal lossless metasurface ($Z_s = j369$ Ω/sq) is able to meet the camouflage condition only in a single-frequency point. Conversely, in the lossy case ($Z_s = R_s + j253$ Ω/sq) shown in Fig. 11(a), a broadband camouflage effect is obtained.

It is worth noticing that the introduction of losses in the metasurface increases the extinction cross section (i.e., the sum of the scattering and absorption cross section) of the coated object. Thus, while lossy metasurfaces allow us to achieve the camouflage effect for the scattering cross section in a broader bandwidth, the extinction cross sections of the targeted object and of the coated one are different. Consequently, the object coated with a lossy metasurface cannot be considered perfectly "camouflaged" since its absorption is different from the expected one. However, there are many applications, as, for example, many radars at microwave frequencies or dark-field microscopies at optical frequencies [34], where the detectability of the object is related only to its scattering. For these scenarios, the lossy metasurface may provide excellent camouflage performance in a broad frequency range.

We conclude this section by observing that the realization of a lossy metasurface is a quite straightforward task, since it can be achieved by exploiting the traditional metasurface designs but replacing metals with lossy materials. Some examples of microwave and optical frequencies are available in Refs. [35,36], respectively.

VI. CONCLUSION

In this paper, we present a systematic approach for camouflaging objects through the use of metasurfaces. In particular, we analytically discuss the scattering manipulation problem for small cylinders and identify the behavior of the surface impedance that is able to transform the scattering of a particle into the one of another particle; i.e., it is able to achieve a camouflage effect. The proposed approach provides a general methodology for transforming the scattering signature of an object in a desired way. We successfully validate the analytical results through a proper set of full-wave simulations. Moreover, an analysis of the frequency performance of the camouflage effect based on the use of passive metasurfaces is investigated, and some solutions to enhance the operative bandwidth are proposed. The concept and the approach presented here for the case of small cylinders can be potentially extended to different geometries using an analytical approach (for canonical shapes) or recurring to semianalytical approximations.

APPENDIX A: DERIVATION OF THE SCATTERING COEFFICIENT b_0'

In the following, we describe the derivation of Eq. (5) according to the notation of Ref. [29]. We know that the magnetic field components of the incident, scattered, and inner fields can be derived from the electric field components reported in Eq. (4), using the relation $\boldsymbol{H}_{i|s|1|m} = -j/\omega\mu_0 \nabla \times \boldsymbol{E}_{i|s|1|m}$, where the expressions of $\mathbf{M}_n^{(1)}(r,\phi,z)$, $\mathbf{N}_n^{(1)}(r,\phi,z)$, $\mathbf{M}_n^{(3)}(r,\phi,z)$, and $\mathbf{N}_n^{(3)}(r,\phi,z)$ in Eq. (4) in cylindrical coordinate are

$$\mathbf{M}_n^{(1)} = \sqrt{k^2-h^2}\left(jn\frac{Z_n^{(1)}(\rho)}{\rho}, -Z_n^{(1)'}(\rho), 0\right)e^{j(n\phi+hz)},$$
$$\mathbf{N}_n^{(1)} = \frac{\sqrt{k^2-h^2}}{k}\left(jhZ_n^{(1)'}(\rho), -hn\frac{Z_n^{(1)}(\rho)}{\rho}, \sqrt{k^2-h^2}Z_n^{(1)}(\rho)\right)e^{j(n\phi+hz)},$$
$$\mathbf{M}_n^{(3)} = \sqrt{k^2-h^2}\left(jn\frac{Z_n^{(3)}(\rho)}{\rho}, -Z_n^{(3)'}(\rho), 0\right)e^{j(n\phi+hz)},$$
$$\mathbf{N}_n^{(3)} = \frac{\sqrt{k^2-h^2}}{k}\left(jhZ_n^{(3)'}(\rho), -hn\frac{Z_n^{(3)}(\rho)}{\rho}, \sqrt{k^2-h^2}Z_n^{(3)}(\rho)\right)e^{j(n\phi+hz)}, \tag{A1}$$

where $h = \cos\zeta$, ζ the angle of incidence (equal to $\pi/2$ for a normally incident TM-plane wave), and Z_n a solution of the cylindrical Bessel equation $\rho(d/d\rho)(\rho(d/d\rho)Z_n) + (\rho^2 - n^2)Z_n = 0$. Thus, the analytical expressions of the electric fields can be in the following form:

$$\boldsymbol{E}_i|_{\rho=k_0 r\sin\zeta}, \qquad \boldsymbol{E}_s|_{\rho=k_0 r\sin\zeta},$$
$$\boldsymbol{E}_1|_{\rho=k_0 r\sqrt{\varepsilon_2-\cos(\zeta)^2}}, \qquad \boldsymbol{E}_m|_{\rho=k_0 r\sin\zeta}.$$

The boundary conditions to be applied at $r = a_2$ and $r = a_c$ are, respectively,

$$\begin{aligned}
\boldsymbol{E}_1^{\tan}|_{\rho=k_0a_2} &= \boldsymbol{E}_{\boldsymbol{m}}^{\tan}|_{\rho=k_0a_2},\\
\boldsymbol{H}_1^{\tan}|_{\rho=k_0a_2} &= \boldsymbol{H}_{\boldsymbol{m}}^{\tan}|_{\rho=k_0a_2},\\
\boldsymbol{E}_{\boldsymbol{m}}^{\tan}|_{\rho=k_0a_c} &= Z_s\hat{\boldsymbol{r}}[(\boldsymbol{H}_{\boldsymbol{i}}^{\tan}|_{\rho=k_0a_c} + \boldsymbol{H}_{\boldsymbol{s}}^{\tan}|_{\rho=k_0a_c})\\
&\quad - \boldsymbol{H}_{\boldsymbol{m}}^{\tan}|_{\rho=k_0a_c}],\\
\boldsymbol{E}_{\boldsymbol{i}}^{\tan}|_{\rho=k_0a_c} + \boldsymbol{E}_{\boldsymbol{s}}^{\tan}|_{\rho=k_0a_c} &= Z_s\hat{\boldsymbol{r}}[(\boldsymbol{H}_{\boldsymbol{i}}^{\tan}|_{\rho=k_0a_c} + \boldsymbol{H}_{\boldsymbol{s}}^{\tan}|_{\rho=k_0a_c})\\
&\quad - \boldsymbol{H}_{\boldsymbol{m}}^{\tan}|_{\rho=k_0a_c}].
\end{aligned} \tag{A2}$$

Please note that, as for an uncoated dielectric cylinder [29], all the scattering coefficients a_n' vanish when the impinging field is normal to the axis of the cylinder. Therefore, the series of the scattering coefficients b_n' can be expressed in the convenient form $b_n' = \boldsymbol{N}/\boldsymbol{D}$ with

$$\begin{aligned}
\boldsymbol{N}&: A_n[jK_nC_n(B_{n-1}C_{-n} + B_{1-n}C_n) + 2Z_sB_{n-1}] + j\sqrt{\varepsilon_2}A_{n-1}[K_nC_n(B_{-n}C_n + B_nC_{-n}) + j2Z_sB_n],\\
\boldsymbol{D}&: \pi a_c[C_n(D_{n-1}A_n - \sqrt{\varepsilon_2}D_nA_{n-1})(\mu_0\omega E_n - jk_0Z_sE_{n-1}) + E_nA_n(-\mu_0\omega B_{n-1}E_n + jk_0Z_sD_{n-1}C_{n-1})\\
&\quad + \sqrt{\varepsilon_2}E_nA_{n-1}(\mu_0\omega B_nE_n - jk_0Z_sD_nC_{n-1})],
\end{aligned} \tag{A3}$$

where $A_n = J_n(a_2k_0\sqrt{\varepsilon_2})$, $B_n = J_n(a_2k_0)$, $C_n = J_n(a_ck_0)$, $D_n = H_n^{(1)}(a_ck_0)$, $E_n = H_n^{(1)}(a_ck_0)$, $K_n = \pi a_c\mu_0\omega\csc(n\pi)$, and $J_n(\cdot)$, $H_n^{(1)}(\cdot)$ are the cylindrical Bessel and Hankel functions of the first kind, respectively.

Assuming that the coated cylinder is electrically small ($n \to 0$), only the first- $(J_0(\cdot), H_0^{(1)}(\cdot))$ and second-order $(J_1(\cdot), H_1^{(1)}(\cdot))$ Bessel and Hankel functions give a significant contribution in Eq. (A3). Thus, $b_0' = \boldsymbol{N}/\boldsymbol{D}$ assumes the following form:

$$\begin{aligned}
\boldsymbol{N}&: (2\sqrt{\varepsilon_2}B_0A_1 - 2B_1A_0)[2jC_0(\mu_0\omega E_0 - jk_0Z_sE_1) - 2k_0Z_sC_0E_0] + 2j\mu_0\omega C_0^2(2D_1A_0 - 2\sqrt{\varepsilon_2}D_0A_1),\\
\boldsymbol{D}&: A_0[-4j\mu_0\omega B_1E_0^2 - 2D_1E_0(-2k_0Z_sC_1 - 2j\mu_0\omega C_0) - 4k_0Z_sD_1C_0E_1]\\
&\quad - 4\sqrt{\varepsilon_2}A_1\left[\frac{1}{2}E_0(2k_0Z_sD_0C_1 - 2j\mu_0\omega B_0E_0) + D_0C_0(-k_0Z_sE_1 + j\mu_0\omega E_0)\right].
\end{aligned} \tag{A4}$$

Introducing the following asymptotic expansion of the Bessel functions for small arguments [30],

$$A_n \to \frac{1}{n!}\left(\frac{a_2k_0\sqrt{\varepsilon_2}}{2}\right)^n, \qquad B_n \to \frac{1}{n!}\left(\frac{a_2k_0}{2}\right)^n, \qquad C_n \to \frac{1}{n!}\left(\frac{a_ck_0}{2}\right)^n,$$
$$D_0 \to j\frac{2}{\pi}\ln(a_2k_0), \qquad D_1 \to -j\frac{1}{\pi}\left(\frac{a_2k_0}{2}\right)^{-1}, \qquad E_0 \to j\frac{2}{\pi}\ln(a_ck_0), \qquad E_1 \to -j\frac{1}{\pi}\left(\frac{a_ck_0}{2}\right)^{-1}, \tag{A5}$$

the expression of the fundamental order scattering coefficient of a coated cylinder b_0' reduces from Eq. (A4) to Eq. (5).

It is worth noticing that the approximations that lead from Eq. (A4) to Eq. (A5) are rigorously valid only if the arguments of the Bessel functions approach zero, i.e., for $a_1k_0, a_ck_0, a_2k_0\sqrt{\varepsilon_2} \to 0$. This is a *stronger* condition compared to the assumption of the *electrically small* object (i.e., $a_1k_0, a_ck_0, a_2k_0\sqrt{\varepsilon_2} \ll 1$) that we employ to derive Eq. (A4). However, we point out that it is possible to derive the camouflage impedance Z_s even without the small-argument approximation. In this case, of course, the closed-form expression is more cumbersome and reads as

$$Z_s = jX_s = j\frac{\pi a_c \mu_0 \omega C_0}{2(\Delta_1 - \Delta_2)},$$
$$\Delta_{k=1,2} = \frac{\sqrt{\varepsilon_k}B_{0,k}A_{1,k} - B_{1,k}A_{0,k}}{B_{1,k}F_0A_{0,k} + \sqrt{\varepsilon_k}A_{1,k}(G_{0,k}C_0 - A_{0,1}F_0) - G_{1,k}C_0A_{0,k}}, \tag{A6}$$

having $A_{n,k}$, $B_{n,k}$ as the same expressions as in Eq. (A3) but replacing the parameters a_2, ε_2 with a_k, ε_k [e.g., $A_{n,k} = J_n(a_k k_0\sqrt{\varepsilon_k})$] and being $F_n = Y_n(a_c k_0)$ and $G_{n,k} = Y_n(a_k k_0)$, where $Y(\cdot)$ is the cylindrical Bessel functions of the second kind.

APPENDIX B: THE APPARENT SECOND CAMOUFLAGE SOLUTION

From Fig. 4, it can be observed that for a given camouflage surface reactance evaluated at f_0 using Eq. (6), a similar value of the SCS is also achieved at another frequency (in this specific case, around $0.86f_0$). This fact can give the mistaken impression that a second camouflage solution also exists.

To better understand this point, we invite the reader to look at Fig. 12, where the values of the fundamental scattering coefficient of the targeted cylinder (b_0) and the coated cylinder (b_0') are reported in both real and imaginary parts as a function of the frequency [Fig. 12(a)] and as a function of the surface impedance of the cover [Fig. 12(b)]. Please note that the geometrical parameters of this case are the same as the ones of the example that we discuss in Sec. III.

As we clarify in the theoretical part of the manuscript, a camouflage condition is achieved when both the real and the imaginary parts of the two scattering coefficients are equal. As it should be clear in Fig. 12, this condition is met only at the designed frequency f_0, i.e., for the value of the surface impedance returned by Eq. (6): $X_s = X_{s1} = -65\ \Omega/\text{sq}$.

The other solution that seems to appear in Fig. 4 is due to the fact that a different frequency also exists (around $0.86f_0$) for which only the absolute value of the two scattering coefficients is the same. For this solution, however, the phase of the scattering coefficient is opposite. Therefore, this second apparent solution is not interesting for camouflage applications because the camouflaged object can still be detectable from the phase distribution of the scattered electromagnetic field that is different from the expected one.

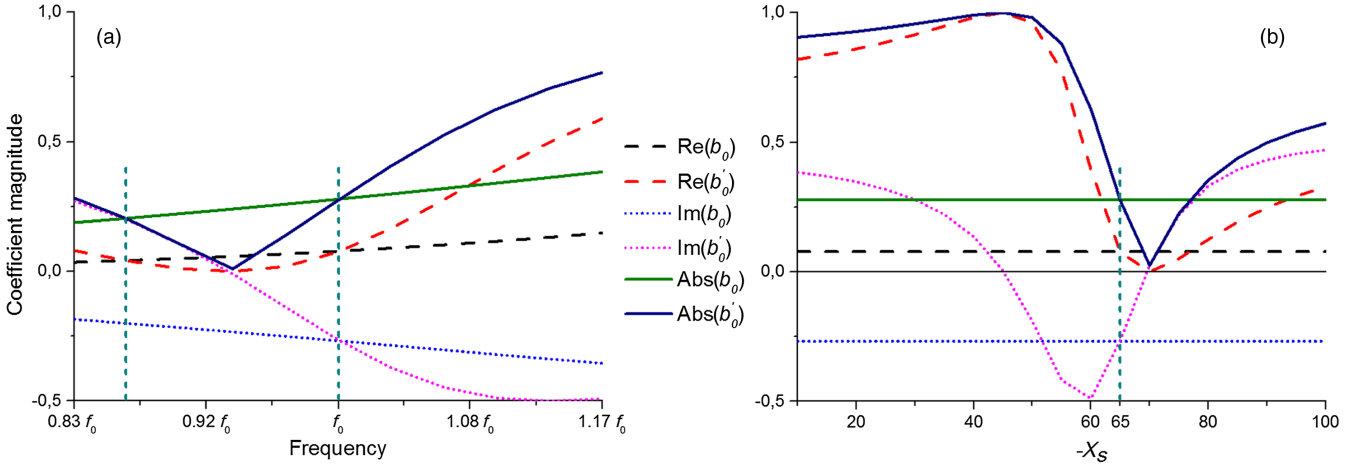

FIG. 12. Comparison between the fundamental scattering coefficient of the coated (b_0') and targeted (b_0) cylinder as (a) the frequency and as (b) the surface impedance X_s of the cover changes.

[1] J. B. Pendry, D. Schurig, and D. R. Smith, Controlling electromagnetic fields, Science **312**, 1780 (2006).

[2] P. Alitalo, O. Luukkonen, L. Jylha, J. Venermo, and S. A. Tretyakov, Transmission-line networks cloaking objects from electromagnetic fields, IEEE Trans. Antennas Propag. **56**, 416 (2008).

[3] A. Alù and N. Engheta, Achieving transparency with plasmonic and metamaterial coatings, Phys. Rev. E **72**, 016623 (2005).

[4] A. Alù, Mantle cloak: Invisibility induced by a surface, Phys. Rev. B **80**, 245115 (2009).

[5] F. Monticone and A. Alù, Invisibility exposed: Physical bounds on passive cloaking, Optica **3**, 718 (2016).

[6] D. Schurig, J. J. Mock, B. J. Justice, S. A. Cummer, J. B. Pendry, A. F. Starr, and D. R. Smith, Metamaterial electromagnetic cloak at microwave frequencies, Science **314**, 977 (2006).

[7] D. Rainwater, A. Kerkhoff, K. Melin, J. C. Soric, G. Moreno, and A. Alù, Experimental verification of three-dimensional plasmonic cloaking in free-space, New J. Phys. **14**, 013054 (2012).

[8] P. Alitalo, F. Bongard, J.-F. Zürcher, J. Mosig, and S. Tretyakov, Experimental verification of broadband cloaking using a volumetric cloak composed of periodically stacked cylindrical transmission-line networks, Appl. Phys. Lett. **94**, 014103 (2009).

[9] A. Monti, J. Soric, A. Alù, F. Bilotti, A. Toscano, and L. Vegni, Overcoming mutual blockage between neighboring dipole antennas using a low-profile patterned metasurface, IEEE Antennas Wireless Propag. Lett. **11**, 1414 (2012).

[10] A. Monti, J. Soric, A. Alù, A. Toscano, and F. Bilotti, Dual-polarized reduction of dipole antenna blockage using mantle cloaks, IEEE Trans. Antennas Propag. **63**, 1775 (2015).

[11] H. M. Bernety and A. B. Yakovlev, Reduction of mutual coupling between neighboring strip dipole antennas using confocal elliptical metasurface cloaks, IEEE Trans. Antennas Propag. **63**, 1554 (2015).

[12] Z. H. Jiang, P. E. Sieber, L. Kang, and D. H. Werner, Restoring intrinsic properties of electromagnetic radiators using ultralightweight integrated metasurface cloaks, Adv. Funct. Mater. **25**, 4708 (2015).

[13] J. C. Soric, A. Monti, A. Toscano, F. Bilotti, and A. Alù, Dual-polarized reduction of dipole antenna blockage using mantle cloaks, IEEE Trans. Antennas Propag. **63**, 4827 (2015).

[14] A. Monti, J. Soric, M. Barbuto, D. Ramaccia, S. Vellucci, F. Trotta, A. Alù, A. Toscano, and F. Bilotti, Mantle cloaking for co-site radio-frequency antennas, Appl. Phys. Lett. **108**, 113502 (2016).

[15] A. Alù and N. Engheta, Cloaking a Sensor, Phys. Rev. Lett. **102**, 233901 (2009).

[16] M. Fruhnert, A. Monti, I. Fernandez-Corbaton, A. Alù, A. Toscano, F. Bilotti, and C. Rockstuhl, Tunable scattering cancellation cloak with plasmonic ellipsoids in the visible, Phys. Rev. B **93**, 245127 (2016).

[17] R. Fleury, F. Monticone, and A. Alù, Invisibility and Cloaking: Origins, Present, and Future Perspectives, Phys. Rev. Applied **4**, 037001 (2015).

[18] Y. R. Padooru, A. B. Yakovlev, P. Y. Chen, and A. Alù, Analytical modeling of conformal mantle cloaks for cylindrical objects using sub-wavelength printed and slotted arrays, J. Appl. Phys. **112**, 034907 (2012).

[19] J. C. Soric, A. Monti, A. Toscano, F. Bilotti, and A. Alù, Multiband and wideband bilayer mantle cloaks, IEEE Trans. Antennas Propag. **63**, 3235 (2015).

[20] P. Y. Chen, M. Farhat, S. Guenneau, S. Enoch, and A. Alù, Acoustic scattering cancellation via ultrathin pseudo-surface, Appl. Phys. Lett. **99**, 191913 (2011).

[21] M. D. Guild, A. Alù, and M. R. Haberman, Cloaking of an acoustic sensor using scattering cancellation, Appl. Phys. Lett. **105**, 023510 (2014).

[22] Y. Lai, J. Ng, H. Y. Chen, D. Z. Han, J. J. Xiao, Z. Q. Zhang, and C. T. Chan, Illusion Optics: The Optical Transformation of an Object into Another Object, Phys. Rev. Lett. **102**, 253902 (2009).

[23] F. Yang, Z. L. Mei, W. X. Jiang, and T. J. Cui, Electromagnetic illusion with isotropic and homogeneous materials through scattering manipulation, J. Opt. **17**, 105610 (2015).

[24] Z. H. Jiang and D. H. Werner, Metasurface-enabled electromagnetic cloaking and illusion coatings beyond the quasi-static limit," in *Proceedings of 2014 IEEE APS International Symposium, Memphis, TN, 2014* (IEEE, New York, 2014).

[25] N. Xiang, Q. Cheng, H. B. Chen, J. Zhao, W. X. Jiang, H. F. Ma, and T. J. Cui, Bifunctional metasurface for electromagnetic cloaking and illusion, Appl. Phys. Express **8**, 092601 (2015).

[26] Z. H. Jiang and D. H. Werner, Quasi-three-dimensional angle-tolerant electromagnetic illusion using ultrathin metasurface coatings, Adv. Funct. Mater. **24**, 7728 (2014).

[27] M. Selvanayagam and G. V. Eleftheriades, Experimental Demonstration of Active Electromagnetic Cloaking, Phys. Rev. X **3**, 041011 (2013).

[28] M. Alaoui, K. Rustomji, T. M. Chang, G. Tayeb, P. Sabouroux, R. Quidant, S. Enoch, S. Guenneau, and R. Abdeddaim, Cyclic concentrator, carpet cloaks and fisheye lens via transformation plasmonics, J. Opt. **18**, 044023 (2016).

[29] C. F. Bohren and D. R. Huffman, *Absorption and Scattering of Light by Small Particles* (John Wiley & Sons, New York, 2008).

[30] M. Abramowitz and I. A. Stegun, *Handbook of Mathematical Functions* (Dover Publications Inc., New York, 1998).

[31] A. Sihvola, P. Yla-Oijala, S. Jarvenpaa, and J. Avelin, Polarizabilities of platonic solids, IEEE Trans. Antennas Propag. **52**, 2226 (2004).

[32] P. Y. Chen, C. Argyropoulos, and A. Alù, Broadening the Cloaking Bandwidth with Non-Foster Metasurfaces, Phys. Rev. Lett. **111**, 233001 (2013).

[33] See https://www.cst.com for CST Microwave Studio 2015.

[34] S. Mühlig, A. Cunningham, J. Dintinger, M. Farhat, S. Bin Hasan, T. Scharf, T. Bürgi, F. Lederer, and C. Rockstuhl, Reply on the comment on "A self-assembled three-dimensional cloak in the visible", Sci. Rep. **3**, 2328 (2013).

[35] H. Mosallaei and K. Sarabandi, A one-layer ultra-thin meta-surface absorber, in *Proceedings of 2005 IEEE APS International Symposium, Washington, D.C., 2005* (IEEE, New York, 2005).

[36] A. Monti, A. Toscano, and F. Bilotti, Exploiting the surface dispersion of nanoparticles to design optical-resistive sheets and Salisbury absorbers, Opt. Lett. **41**, 3383 (2016).